JOURNAL OF AIRCRAFT
Vol. 45, No. 3, May–June 2008

Delta Wing with Store Limit-Cycle-Oscillation Modeling Using a High-Fidelity Structural Model

Peter J. Attar*
University of Oklahoma, Norman, Oklahoma 73019
and
Earl H. Dowell† and Deman Tang‡
Duke University, Durham, North Carolina 27708-0300

DOI: 10.2514/1.32217

The flutter and limit-cycle oscillation behavior of a 45-deg delta-wing-store model with various store spanwise locations is studied using an aeroelastic model that includes a high-fidelity nonlinear finite element structural solver and a vortex-lattice aerodynamic model. The store aerodynamics are modeled using slender-body theory. The computed results are compared with a previous computational model and with the experiment. The zero-angle-of-attack flutter behavior of the wing-store configuration is shown to be sensitive to the spanwise store location. This is predicted accurately using the current methodology. Limit-cycle oscillation results for zero angle of attack are computed for two store spanwise locations and compare favorably with the experiment. For a clean-wing configuration and a configuration that had the store located at $y/c = 0.291$, the flutter results show very little sensitivity to the model angle of attack. This too was predicted accurately using the current model. However, when the store is placed at $y/c = 0.545$, the experimental flutter data show a large sensitivity to angle of attack, with the flutter velocity decreasing by almost 20% when the model is placed at an angle of attack of 2 deg. This is not predicted in the current work and it is possible that unmodeled flow physics such as leading-edge vortices are the cause of this difference.

I. Introduction

MODERN high-performance aircraft often are required to operate with numerous wing-store configurations. The presence of stores can often induce flutter at flow conditions for which the clean-wing configuration would exhibit stability. A limited-amplitude motion, often referred to as a limit-cycle oscillation (LCO), can occur if a nonlinear mechanism in the system is strong enough to limit the exponential growth in amplitude predicted by a linear aeroelastic model of the flutter condition. The nonlinearities that are important for a given occurrence of a limit-cycle oscillation can be structural, fluid, or both.

A good deal of work in the last decade has looked at the limit-cycle oscillations of clean-wing configurations. In work done by Tang et al. [1,2], it was shown through theory and experiment that a limit cycle can be caused by a structural nonlinearity alone. In that work, a nonlinear structural model was coupled to a linear vortex lattice to look at the dynamic behavior of thin-plate wings in low subsonic flow. Attar et al. [3] extended the work of [1,2] to include a more accurate theoretical structural model that achieved a better correlation with the experiment for both zero and nonzero-angle-of-attack flutter parameters and the LCO magnitudes.

In work that looked at LCO at higher transonic Mach numbers ($M \approx 0.8$), Gordnier [4] studied the LCO of a cropped flat-plate delta wing. In that work, viscous effects were found to be of little importance for the Mach range studied, because the numerical results from a Navier–Stokes solution and an Euler solution were comparable. A finite element solution of the nonlinear von Kármán plate model was used to model the structural behavior.

The LCO of two-dimensional airfoils and three-dimensional wings in transonic flow has been studied using various reduced-order methods [5–11]. In the aeroelastic models used in these studies, all of the modeled nonlinearities were contained in the fluid. In recent work by Thomas et al. [11], the effect of stores was included in the computation of the linear modal parameters of the structure; however, the effect of the store aerodynamics was not studied.

Beran et al. [12] studied the effect of the fluid modeling fidelity on the LCO of wings with and without stores. In that work, a linear modal structural model was used in combination with several different fluid models. They found that including higher-order fluid effects did change the predicted flutter/LCO behavior. They also noted that including the wing-store aerodynamics in the model had an effect on the flutter behavior of the system. These calculations were done for Mach numbers in the transonic range.

In work by Kim and Strganac [13], the LCO of a cantilevered wing with stores was modeled using a nonlinear beam model that included both kinematic and geometric nonlinearities. The aerodynamic model used was a nonlinear quasi-steady model with a subsonic stall model. In that work, they found that the structural geometric nonlinearity played a vital part in the wing undergoing subcritical LCO. Less important was the role of the kinematic nonlinearity due to the mass imbalance. Further study by these authors included the study of the wing-store limit-cycle behavior using a nonlinear beam coupled to a transonic small-disturbance fluid solver [14].

Numerous studies [15–18] have been conducted on wing-store limit-cycle oscillations. Recent work has focused on the effect that nonlinear damping plays in the limit-cycle behavior [17,18].

In work that is most similar to the work presented here, Tang et al. [19] studied, both experimentally and numerically, the LCO of a wing-store model for various store placements. A nonlinear von Kármán plate model was used with a component-mode method to model the structural behavior of the wing-store system. A linear reduced-order vortex-lattice aerodynamic model was used for the

Presented as Paper 1913 at the 46th AIAA/ASME/ASCE/AHS/ASC Structures, Structural Dynamics, and Materials Conference, Austin, TX, 18–21 April 2005; received 17 May 2007; accepted for publication 20 December 2007.

*Assistant Professor, Department of Aerospace and Mechanical Engineering, 865 Asp Avenue, Felgar Hall Room 212; peter.attar@ou.edu. Member AIAA.

†William Holland Hall Professor, Department of Mechanical Engineering and Materials Science, Box 90300, Hudson Hall; Dean Emeritus, Pratt School of Engineering. Honorary Fellow AIAA.

‡Research Associate Professor, Department of Mechanical Engineering and Materials Science, Box 90300, Hudson Hall. Member AIAA.

wing aerodynamics, and slender-body theory was used to compute the lift and moment effects from the store. In that work, they found that the inclusion of the store aerodynamics had very little effect on the flutter parameters of the system. However, a large effect was noted due to the placement of the store on the resulting flutter speed. Although the flutter characteristics were predicted accurately in that work, the nonlinear plate model used proved to be inadequate for the accurate prediction of postflutter LCO behavior.

In the work presented here, the LCO of a cantilevered delta-wing/store model is studied using a high-fidelity structural model for both zero and nonzero angles of attacks. The numerical results are compared with the experimental results from [19] and also with some new experimental results. The theoretical model consists of the high-fidelity nonlinear structural model used in [3] coupled to a vortex-lattice aerodynamic model for the wing and slender-body theory for the store.

II. Theory

A. Structural Model

The ANSYS commercial finite element code [20] is used as the nonlinear structural solver in this work. This code uses the principle of virtual work in combination with a Rayleigh–Ritz solution in the form of finite element analysis to develop a system of nonlinear differential equations. The general form of the equations in matrix notation is

$$\mathbf{M}\ddot{\mathbf{U}} + \mathbf{C}\dot{\mathbf{U}} + \mathbf{K}\mathbf{U} = \mathbf{F} \tag{1}$$

where $\mathbf{U}$ is the vector of nodal degrees of freedom; $\mathbf{M}$, $\mathbf{C}$, and $\mathbf{K}$ are the mass, damping, and stiffness matrices, respectively; and $\mathbf{F}$ is the vector of applied loads (which, in this analysis, are due to pressure on the wing and point moments and forces due to the store aerodynamic forces). Note that because geometric nonlinearities are to be included in this analysis, the stiffness matrix is a function of the nodal displacements. Also, a Rayleigh damping model is used here, and so the damping matrix $\mathbf{C}$ is written as a linear combination of the mass and stiffness matrices.

The geometric nonlinearity due to large deflection and large rotation is modeled in the ANSYS code using a corotational approach. In this method, a local coordinate system is attached to each element that rotates and translates with the element as deformation takes place. The original element coordinate system stays fixed and the element deformation can therefore be decomposed into a component due to rigid-body motion and a component that induces strain. This decomposition is applied using a matrix transformation:

$$\mathbf{B}_l = \mathbf{B}\mathbf{T}_l \tag{2}$$

where $\mathbf{B}$ is the strain-displacement matrix in the original element coordinates, $\mathbf{B}_l$ is the strain-displacement matrix written in the local coordinate system, and $\mathbf{T}_l$ is the orthogonal transformation matrix that relates the original element coordinates to the local coordinates. Note that linear strain-displacement relationships are used in the preceding matrix $\mathbf{B}$.

A second type of geometric nonlinearity that is included in the model is stress-stiffening. Stress-stiffening takes into account the coupling of the in-plane and out-of-plane displacements. This coupling causes membrane forces to have an influence on the out-of-plane deflection of a structure. This effect is especially important for structures in which the bending stiffness is much smaller than the membrane stiffness. In ANSYS, stress-stiffening effects are accounted for using the nonlinear Green strain-displacement relationships:

$$\epsilon_x = \frac{\partial U_x}{\partial x} + \frac{1}{2}\left[\left(\frac{\partial U_x}{\partial x}\right)^2 + \left(\frac{\partial U_y}{\partial x}\right)^2 + \left(\frac{\partial U_z}{\partial x}\right)^2\right] \tag{3}$$

$$\epsilon_y = \frac{\partial U_y}{\partial y} + \frac{1}{2}\left[\left(\frac{\partial U_x}{\partial y}\right)^2 + \left(\frac{\partial U_y}{\partial y}\right)^2 + \left(\frac{\partial U_z}{\partial y}\right)^2\right] \tag{4}$$

$$\gamma_{xy} = \frac{\partial U_x}{\partial y} + \frac{\partial U_y}{\partial x} + \left[\frac{\partial U_x}{\partial x}\frac{\partial U_x}{\partial y} + \frac{\partial U_y}{\partial x}\frac{\partial U_y}{\partial y} + \frac{\partial U_z}{\partial x}\frac{\partial U_z}{\partial y}\right] \tag{5}$$

In ANSYS, the elemental tangent stiffness matrix $\mathbf{K}_{\text{el}}$ is computed using a consistent approach first developed by Nour-Omid and Rankin [21]. In that method, the elemental force vector $\mathbf{F}_{\text{int}}$, which is due to strain energy, is written as the gradient of the strain energy V with respect to the nodal displacements:

$$\mathbf{F}_{\text{int}} = \frac{\partial V}{\partial \mathbf{U}} = \int_{V_{el}} \sigma \, \mathrm{d}V \tag{6}$$

where σ is the vector of elemental stresses and V_{el} is the elemental volume. The tangent stiffness matrix, rotated to the original element coordinates, can now be computed by taking the derivative of Eq. (6) with respect to the nodal displacements:

$$\begin{aligned}\mathbf{K}_{\text{el}}^T &= \mathbf{T}_l^T \frac{\partial \mathbf{F}_{\text{int}}}{\partial \mathbf{U}} + \frac{\partial \mathbf{T}_l^T}{\partial \mathbf{U}}\mathbf{F}_{\text{int}} \\ &= \mathbf{T}_l^T \int_{V_{\text{el}}} \mathbf{B}^T \frac{\partial \sigma}{\partial \mathbf{U}} \, \mathrm{d}V + \mathbf{T}_l^T \int_{V_{\text{el}}} \frac{\partial \mathbf{B}^T}{\partial \mathbf{U}} dV + \frac{\partial \mathbf{T}_l}{\partial \mathbf{U}} \int_{V_{\text{el}}} \mathbf{B}^T \sigma \, \mathrm{d}V\end{aligned} \tag{7}$$

The first integral in Eq. (7) is the main tangent stiffness matrix, and the second and third integrals are due to stress-stiffening. The full-structure-sized stiffness matrix used in Eq. (1) is assembled from the elemental stiffnesses in the usual manner.

In the work presented here, four types of elements are used to discretize the structure: 1) four-node shell element, 2) two-node beam element, 3) point-mass element, and 4) multipoint-constraint element. The beam, mass, and multipoint-constraint elements were used to model the store, and the flexible wing was modeled using the shell elements. See [20] for details on the interpolating functions used for each of these elements.

A more detailed description of how these elements are used will be given in the next section of this paper.

1. Finite Element Model

In Sec. II.A, theoretical details were presented for the nonlinear finite element model used in this work. In finite element analysis, the computational domain is split into subdomains (finite elements). In each of these elements, the spatial variations of the structural field quantities (displacements) are approximated using interpolation functions. The types of interpolation functions used depend on the dimensionality and underlying physics of the problem.

The experimental wing-store model (shown in Fig. 1) is modeled using both flexible and rigid computational components. These can be identified in Fig. 2. The flexible portions of the structure consist of the flat-plate wing structure and the spring (k_s in Fig. 2). In the wind-tunnel model (and in the current finite element model) the spring is a thin flexible beam. The rigid components consist of the store and the rigid attachment that connects the spring/beam to the plate structure. These two rigid components are denoted as $M1$ and $M2$ in Fig. 2.

In the computational model, the flexible delta-wing plate structure is modeled using four-node shell elements (ANSYS SHELL63). This element has six degrees of freedom (three displacements and three rotations) at each node. The flexible beam is modeled using a two-node, three-dimensional beam element (ANSYS BEAM4) with six degrees of freedom at each node. The point masses $M1$ and $M2$ are modeled using a point-mass element (ANSYS MASS21) with six degrees of freedom per node. The rigid portion of the store is modeled with two multipoint-constraint elements (ANSYS MPC184). The rigid connection of point P1 to the rigid store is modeled using constraint equations that force the displacements and two of the rotations (θ_x and θ_z) of the store at the attachment point to be equal to that of point P1 on the flexible wing. The y rotation θ_y is not constrained as the store model rotates about this point. The rigid connection of point P2 to the flexible beam is also modeled using constraint equations, but all rotations and displacements are

constrained here. See Fig. 3 for a graphical depiction of the computational model used in this work.

B. Vortex-Lattice Aerodynamic Model

The flowfield about the delta-wing model is low subsonic flow and is assumed to be a potential flow. Therefore, the equations of motion can be reduced to Laplace's equation:

$$\nabla^2\Phi = 0 \tag{8}$$

The boundary conditions that must be satisfied are that flow at the surface of the wing must be tangent to the wing

$$\nabla\Phi \cdot \mathbf{n} = 0 \tag{9}$$

and that the disturbance created by the velocity potential must decay at large distances from the wing, which can be expressed as

$$\lim_{r\to\infty}(\nabla\Phi - \mathbf{q}) = 0 \tag{10}$$

where $\mathbf{q}$ is the relative velocity between the undisturbed fluid in the fluid domain and the wing. Using a Green's identity, it can be shown [22] that a solution to Eq. (8) can be found by distributing elementary solutions to Laplace's equation on the problem boundaries. For the model presented here, this is accomplished by distributing vortex rings on the wing surface and in the wake.

If the solid boundary of the wing is defined as

$$F(x, y, z, t) = z - \eta(x, y, t) = 0 \tag{11}$$

then Eq. (9) can be expressed as

$$\frac{\mathrm{D}F}{\mathrm{D}t} = \frac{\partial F}{\partial t} - \mathbf{Q}_\infty \cdot \nabla F + \nabla\Phi \cdot \nabla F = 0 \tag{12}$$

where $\mathbf{Q}_\infty = \{U_\infty, V_\infty, W_\infty\}$ is the freestream velocity vector of the wing as viewed from the inertial frame. For the thin surface with zero initial curvature considered here, $\eta(x, y, t)$ can simply be thought of as the out-of-plane structural deformation of the surface

$$\eta(x, y, t) = U_z(x, y, t) \tag{13}$$

If the small-disturbance approximation to the aerodynamic boundary condition is used with Eq. (13), Eq. (12) can be rewritten in the following form:

$$\frac{\partial\Phi}{\partial z} = U_\infty\left(\alpha - \frac{\partial U_z}{\partial x}\right) + \frac{\partial U_z}{\partial t} \tag{14}$$

where the angle α is the angle that the freestream velocity $\mathbf{Q}_\infty$ makes with the x axis.

Equation (14) is discretized by placing vortex rings on the wing and in the wake. The wake is assumed to be planar so that the force-free wake condition is not imposed. This is usually a valid assumption for simulations involving the translation of a fixed wing and using this assumption dramatically increases the computational efficiency of the model. After the discretization, Eq. (14) can be expressed in matrix form as

$$\mathbf{A}_b\Gamma_b^{n+1} = \mathbf{ET}\left[\frac{\partial\mathbf{U}_z}{\partial t} + \frac{\partial\mathbf{U}_z}{\partial x}\right]^{n+1/2} + U_\infty\alpha - \mathbf{A}_w\Gamma_w^n \tag{15}$$

where $\mathbf{A}_b$ is the aerodynamic influence coefficient matrix for the influence of the wing bound circulation at the wing collocation points, $\mathbf{A}_w$ is the influence coefficient matrix for the influence of the wake circulation at the wing collocation points, and Γ_b and Γ_w are the vectors of bound and wake circulation, respectively. Also, the superscripts n and $n+1$ represent the n and $n+1$ physical time steps in the time integration, and $n+1/2$ represents an intermediate step during the fluid–structure subiteration. Finally, $\mathbf{ET}$ is a matrix that interpolates the vector of out-of-plane displacements $\mathbf{U}_z$ from the structural-model nodes to the aerodynamic-model collocation points. This interpolation is performed using a thin-plate spline. See Katz and Plotkin [23] for details on the use of vortex rings to discretize Eq. (14).

The pressure on the wing is computed using a linearized unsteady form of Bernoulli's equation:

$$p_\infty - p = \rho_\infty\left(U_\infty\frac{\partial\Phi}{\partial x} + \frac{\partial\Phi}{\partial t}\right) \tag{16}$$

C. Slender-Body Theory

The simulated store used in this work is slender enough such that the slender-body method of computing lift and moment can be used. See Fig. 1 for a picture of the wing-store experimental model. Note that the interaction between the wing and store aerodynamics is neglected here. The slender-body theory presented in this section follows that put forth by Bisplinghoff et al. [24]. For a rigid body undergoing pitch and plunge motion, the vertical displacement of any point on the body can be written as

$$z_a = -h(t) - \alpha(t)[x_\beta - e1] \tag{17}$$

where z_a is the vertical displacement; $h(t)$ is the plunge motion defined as positive up; $\alpha(t)$ is the angle the store makes, with incoming flow defined as positive nose up; x_β is the chordwise measure of position along the body axis; and $e1$ is the distance to the elastic axis as measured from the leading edge. If the local incidence of the store axis is assumed to be small at all points along the axis, the z-direction velocity of any cross section w_a can be written in the following way:

$$w_a = \frac{\partial z_a}{\partial t} + U_\infty\frac{\partial z_a}{\partial x_\beta} \tag{18}$$

If Eq. (18) is used with the expression for the z momentum of the fluid I_z [24], an expression for the x_β derivative of lift, $\mathrm{d}L/\mathrm{d}x_\beta$ can be written as follows:

$$\frac{\mathrm{d}L}{\mathrm{d}x_\beta} = -\frac{\mathrm{D}}{\mathrm{D}t}\left[\frac{\mathrm{d}I_z}{\mathrm{d}x_\beta}\right] = -\rho_\infty\frac{\mathrm{D}S}{\mathrm{D}t}\left[\frac{\partial z_a}{\partial t} + U_\infty\frac{\partial z_a}{\partial x_\beta}\right] - \rho_\infty S\left[\frac{\mathrm{D}}{\mathrm{D}t}\left(\frac{\partial z_a}{\partial t}\right) + U_\infty\frac{\mathrm{D}}{\mathrm{D}t}\left(\frac{\partial z_a}{\partial x_\beta}\right)\right] \tag{19}$$

where $\mathrm{D}/\mathrm{D}t$ is the substantial derivative, and S is the cross-sectional area (which is equal to πR^2 for a circular cross section of radius R).

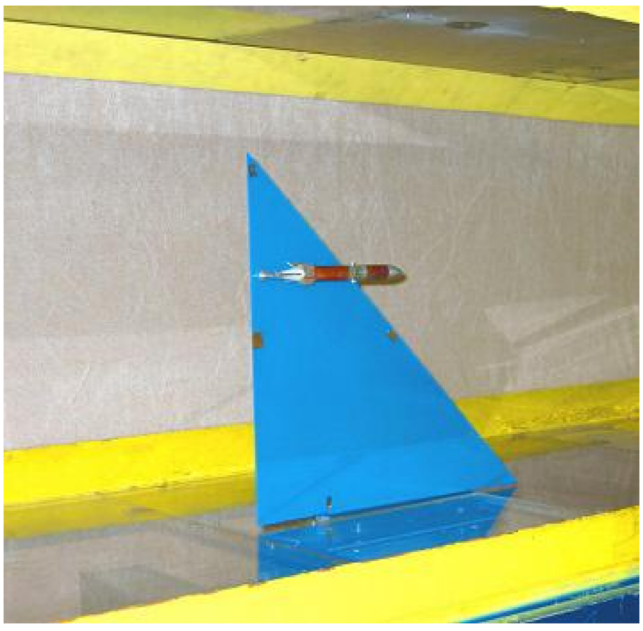

Fig. 1 Photograph of the delta-wing-store wind-tunnel model.

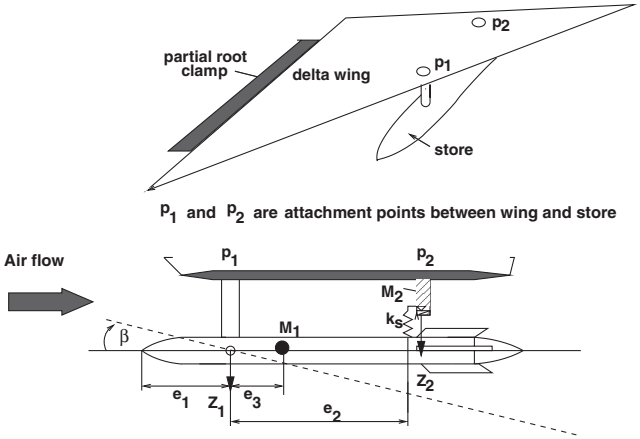

Fig. 2 Schematic of the delta-wing-store model.

If the cross-sectional area is assumed to not change with time such that $\mathrm{D}S/\mathrm{D}t = U_\infty(\mathrm{d}S/\mathrm{d}x_\beta)$, Eq. (19) reduces to

$$\frac{\mathrm{d}L}{\mathrm{d}x_\beta} = -\rho_\infty U_\infty \frac{\mathrm{d}S}{\mathrm{d}x_\beta}\frac{\mathrm{D}z_a}{\mathrm{D}t} - \rho_\infty S\frac{\mathrm{D}^2 z_a}{\mathrm{D}t^2} \tag{20}$$

The total lift on the slender body can be found by integrating Eq. (20) along the full chord length c_{SB}:

$$L = \int_0^{c_{\mathrm{SB}}} \frac{\mathrm{d}L}{\mathrm{d}x_\beta}\,\mathrm{d}x_\beta = \rho_\infty[\ddot{h} + U_\infty\dot{\alpha}(t)]\int_0^{c_{\mathrm{SB}}} S\,\mathrm{d}x_\beta + \rho_\infty\ddot{\alpha}(t)\int_0^{c_{\mathrm{SB}}} S[x_\beta - e1]\,\mathrm{d}x_\beta \tag{21}$$

and the moment about the y axis can be written in the following manner:

$$M_y = \rho_\infty U_\infty[\dot{h}(t) + U_\infty\alpha(t)]\int_0^{c_{\mathrm{SB}}} S\,\mathrm{d}x_\beta - \rho_\infty\ddot{h}(t)\int_0^{c_{\mathrm{SB}}} s[x_\beta - e1]\,\mathrm{d}x_\beta \tag{22}$$

$$- \rho_\infty\ddot{\alpha}(t)\int_0^{c_{\mathrm{SB}}} S[x_\beta - e1]^2\,\mathrm{d}x_\beta \tag{23}$$

where the following relationships were used in Eq. (23):

$$\frac{\mathrm{D}z_a}{\mathrm{D}t} = -\dot{h}(t) - \dot{\alpha}(t)[x_\beta - e1] - U_\infty\alpha(t) \tag{24}$$

$$\frac{\mathrm{D}^2 z}{\mathrm{D}t^2} = -\ddot{h}(t) - \ddot{\alpha}(t)[x_\beta - e1] - 2U_\infty\dot{\alpha} \tag{25}$$

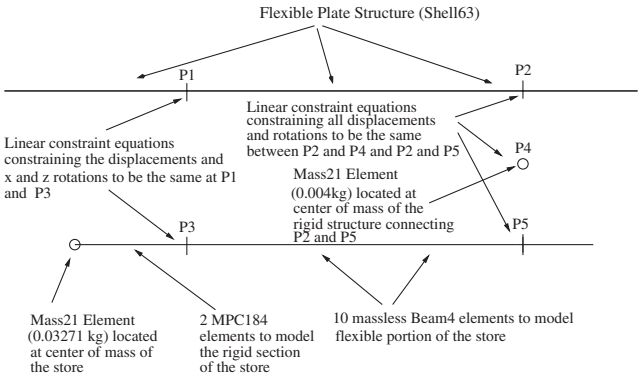

Fig. 3 Schematic of the various elements of the computational model.

D. Fluid–Structure Coupling

To model the aeroelastic phenomena, the structural model and aerodynamic model must be coupled. In the structural equation (1), this coupling is due to the load vector $\{F\}$. In the aerodynamic system, the coupling comes from the x and t derivatives of the out-of-plane deflection U_z in the zero through flow aerodynamic boundary-condition equation (14). To couple the two physics models, both pressure and displacements must be transferred between the aerodynamic model and structural model. This transfer is accomplished using the user-programmable features of ANSYS, which supply subroutines for transferring data between the ANSYS code and a third-party software.

Because the aerodynamic and structural meshes are not necessarily the same, the displacement, velocity, and pressure must be interpolated from one mesh to the other. In the work presented here, the velocities and displacements are interpolated from the structural mesh to the aerodynamic mesh using a thin-plate-spline routine. The pressures are interpolated by finding the best triangle of points on the aerodynamic mesh that contains the structural mesh node to which the pressure value is to be interpolated and then using linear interpolation inside this triangle.

Each time step begins with the prediction of the structural displacement and structural velocity using a Taylor series. These predicted values are used in Eq. (15), and the bound circulation on the wing can then be solved for. Using this circulation, the pressure distribution on the wing can be determined using Eq. (16). This pressure is then passed to ANSYS, which calculates new displacements and velocities. The procedure of recalculating pressure displacements and velocities is continued until the difference in the values for each of the transferred quantities is less than some prescribed tolerance for two successive iterations. Once this is accomplished, the wake is convected and a new time step is taken. The process of subiterating the fluid and structural solutions reduces any temporal lag that may have existed due to the loose coupling of the structural and fluid models and achieves complete synchronization of the equation sets. The importance of synchronizing the loosely coupled systems was demonstrated in the work of Gordnier and Visbal [25].

III. Results

In this work, the flutter and LCO behavior of the wing-store model shown in Figs. 1 and 2 is modeled using the computational model presented in Sec. II and the results are compared with the experiment and to the previous computational work performed in [19]. The delta wing is constructed of 1.47-mm-thick Plexiglas material and has a 45-deg leading-edge sweep. No attempt was made to round the edges of the experimental model. The material density and elastic modulus used in the computational model are 1299 $\mathrm{kg/m^3}$ and 3.3×10^9 Pa, respectively. The middle 60% of the wing root chord is assumed to have a clamped boundary condition.

The values for the various dimensions denoted in Fig. 2 are $e_2 = 9.84$ cm, $e1 = 12.7$ cm, $e3 = -0.23$ cm, $M_1 = 0.037$ kg, and $M_2 = 0.004$ kg. The integrals from Eqs. (21) and (23) are

$$\int_0^{c_{\mathrm{SB}}} S\,\mathrm{d}x_\beta = 2.714 \times 10^{-5}\ \mathrm{m^3}$$

$$\int_0^{c_{\mathrm{SB}}} S[x_\beta - e1]\,\mathrm{d}x_\beta = 3.941 \times 10^{-8}\ \mathrm{m^4}$$

and

$$\int_0^{c_{\mathrm{SB}}} S[x_\beta - e1]^2\,\mathrm{d}x_\beta = 8.38 \times 10^{-9}\ \mathrm{m^5}$$

The structural finite element model consisted of 663 elements: 2 point-mass elements, 10 beam elements, 649 shell elements, and 2 multipoint-constraint elements. The aerodynamic model consisted of 525 vortex rings. The wing wake was assumed to be planar with a

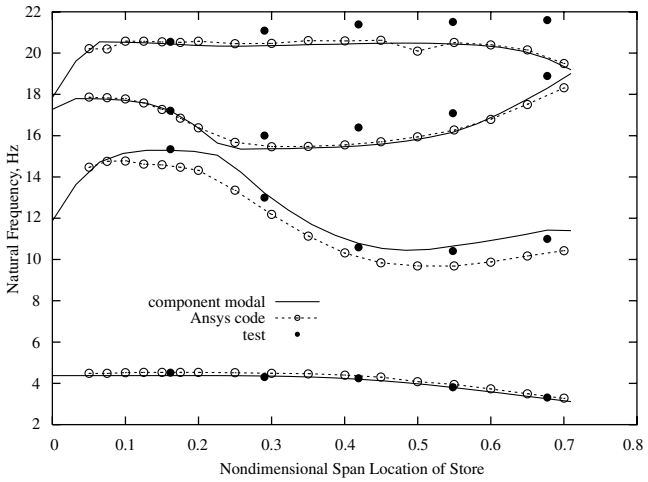

Fig. 4 The first four wing-store modal frequencies plotted vs the normalized y/c store span location.

length of four wing chords. The structural, aerodynamic, and coupling time step used in the simulation was 0.001 s.

A. Flutter: Zero Angle of Attack

The effect of the spanwise location of the store on the wing-store-model flutter velocities and frequencies was investigated. Figure 4 is a plot of the first four modal frequencies of the wing-store model vs the normalized (by the chord) spanwise location of the store. Results are presented for the current computational model, the computational model of [19], and the experiment. All three sets of results agree well over the range of store placements. Figures 5–8 are plots of the first four modes of wing-store model for a store placement of $y/c = 0.545$. Shown in each of the figures are the contour plots of the flexible-wing out-of-plane z mode (5a, 6a, 7a, and 8a) and the out-of-plane mode shape for the store model (5b, 6b, 7b, and 8b). From the figures, one can see that the first mode is primarily the first wing-bending mode. The second mode is primarily the first wing-torsion mode, and the third mode is dominated by the store pitching motion (z deflection of the store). The frequency of the third mode (for the store location of $y/c = 0.545$) is 16.3 Hz, which is very close to the frequency of the uncoupled store pitch mode of 15.5 Hz. The fourth mode is primarily the second wing-bending mode. The effect of moving the store toward the wing tip is reflected the most in the second mode, which, as already mentioned, is primarily the first wing-torsion mode. This is important when one considers that the type of flutter that is typical in the subsonic region for fixed-wing configurations is a coalescence flutter involving the first wing bending and first wing-torsion modes. In Fig. 9, the flutter velocity and flutter frequency for the wing-store model at zero angle of attack are plotted as a function of the normalized store placement location y/c. The computational results in this figure are taken from [19]. The current model results agree well with both the experiment and the results from [19]. This figure shows that the zero-angle-of-attack flutter results are quite sensitive to the spanwise location of the store. Note, however, that although the flutter velocity and flutter frequency do change significantly with the spanwise location of the store, the flutter mode is essentially a coupled bending-torsion motion, regardless of the placement of the store.

B. Flutter: Nonzero Angle of Attack

Previous investigations into the flutter and LCO behavior of clean delta-wing configurations showed that placing the wing at an angle of attack had very little effect on the flutter velocity and frequency of the models [26,27]. In [27], it was noted that placing the wing at an angle of attack of 4 deg resulted in less than a 10% increase in the flutter velocity of the model. The computational model used in that study (similar to the one used here) predicted a similar trend in the flutter velocity as a function of angle of attack. The small changes in flutter velocity and flutter frequency induced by the change in angle of attack for these models were more than likely caused by a slight stiffening of the wing due to the static deflection of the wing and the

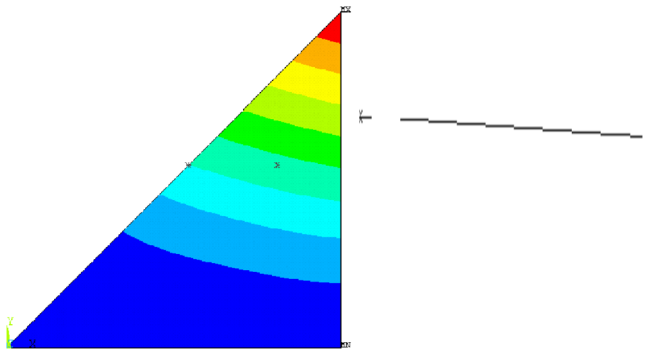

Fig. 5 Mode 1, $y/c = 0.545$: a) flexible-wing out-of-plane z displacement contour and b) close-up view of store out-of-plane displacement.

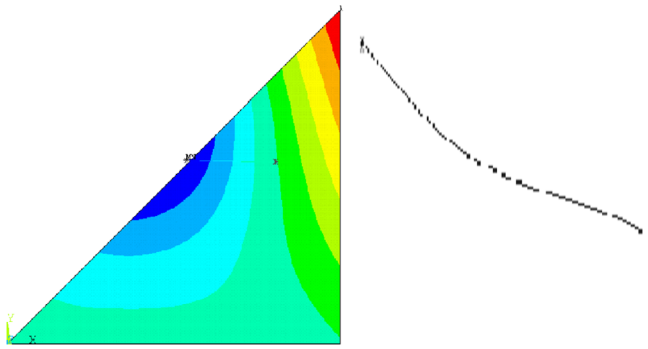

Fig. 6 Mode 2, $y/c = 0.545$: a) flexible-wing out-of-plane z displacement contour and b) close-up view of store out-of-plane displacement.

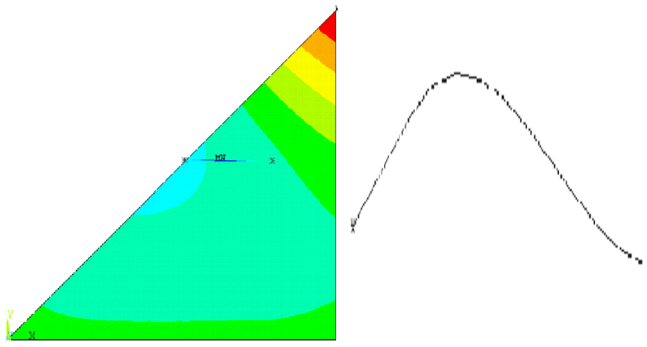

Fig. 7 Mode 3, $y/c = 0.545$: a) flexible-wing out-of-plane z displacement contour and b) close-up view of store out-of-plane displacement.

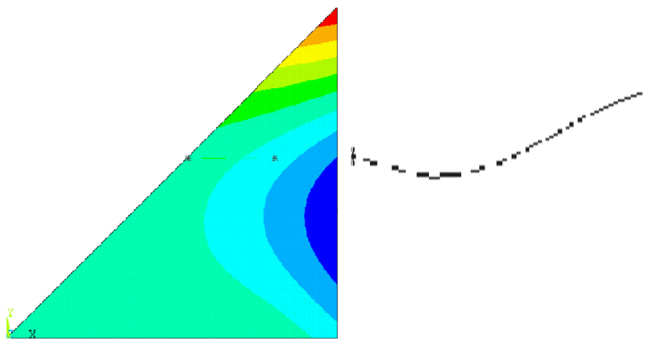

Fig. 8 Mode 4, $y/c = 0.545$: a) flexible-wing out-of-plane z displacement contour and b) close-up view of store out-of-plane displacement.

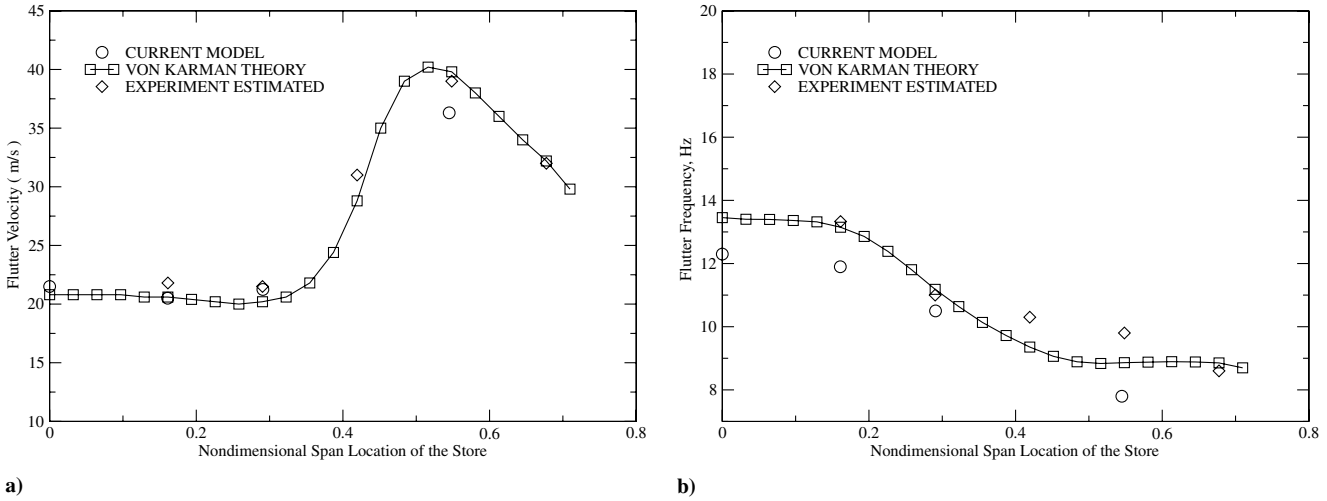

Fig. 9 Wing-store-model flutter results: a) flutter velocity vs store placement and b) flutter frequency vs store placement.

geometric nonlinearities in the structure. This stiffening effectively changes the modes of the model, which in turn will change the flutter behavior. The behavior is similar to that seen in Figs. 4 and 9, in which it was noted that changing the model's modal frequencies by moving the location of the store changed the flutter behavior of the model. However, for the partially cantilevered clean-wing configurations used in the previous studies, the strength of the geometric nonlinearity was fairly weak, which resulted in only a small change in the flutter behavior at nonzero angles of attack.

Figure 10 is a plot of the wing-store-model flutter velocity as a function of angle of attack. Shown in the figure are the results computed using the current model and those measured in the experiment. Three different store configurations are shown 1) clean-wing configuration 2) store attached at $y/c = 0.291$, and 3) store attached at $y/c = 0.545$. The trends of flutter velocity vs angle of attack for the clean-wing case and for the case in which the store is located at $y/c = 0.291$ are very similar to those computed and measured in the previously mentioned studies. Very little change in the flutter velocity is measured (and computed) with a change in the angle of attack. Note that computed results for the clean-wing configuration are symmetric with respect an angle of attack of zero, but the experimental results are not. The reason for this is more than likely due to some small initial curvature in the experimental model. Unlike the other two store configurations, the model that has the store attached at $y/c = 0.545$ appears to be very sensitive to changes in angle of attack. An almost 20% change (when compared with the zero-angle-of-attack case) in flutter velocity is measured in the experimental model when the wing is placed at an angle of attack of 2 deg.

Although this behavior has not been noted in other configurations previously investigated, if Fig. 9 is taken into consideration, the results may not be surprising. From Fig. 9a, it is clear that when the store is located near $y/c = 0.545$, a fairly small movement of the store in either the inboard or outboard direction causes a large decrease in the flutter velocity. One might then expect that placing the wing at an angle of attack could change the wing's modal characteristics and/or flow dynamics in such a way as to mimic an inboard or outboard movement of the store. Unfortunately, this behavior is not predicted by the current computational model. Although nonlinear structural effects brought about by a static deflection should be properly modeled with the current computational method (see Figs. 11–14 for a comparison of the measured and computed static deflections of the wing-store model with the store placed at $y/c = 0.545$), nonlinear aerodynamic effects are not modeled here. It is possible that to properly predict this sensitivity to an angle of attack for this store location, nonlinear aerodynamic effects such as the formation of a leading-edge vortex need to be considered.

C. Limit-Cycle Oscillations

Figure 15 is a plot of the delta-wing LCO tip velocity as a function of flow velocity for a store location of $y/c = 0.161$. The wing was placed at zero angle of attack. Shown on the plot are the theoretical results computed using the computational model of the current work, along with those from [19]. The theoretical results are also compared with those from the experiment. As can be seen, the higher-order structural theory and von Kármán model predict similar flutter

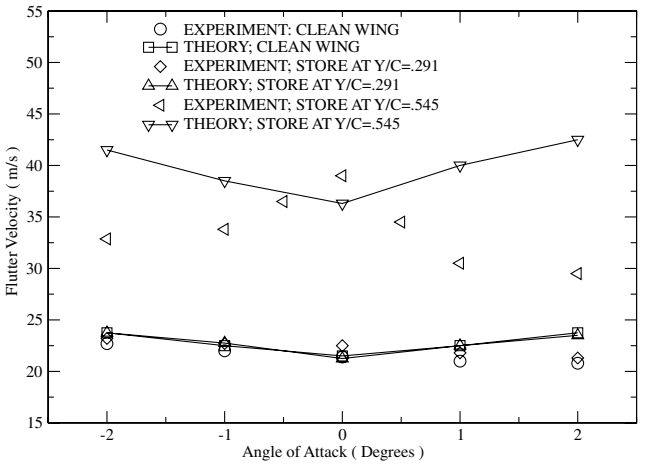

Fig. 10 Delta-wing flutter velocity as a function of angle of attack for three different store configurations.

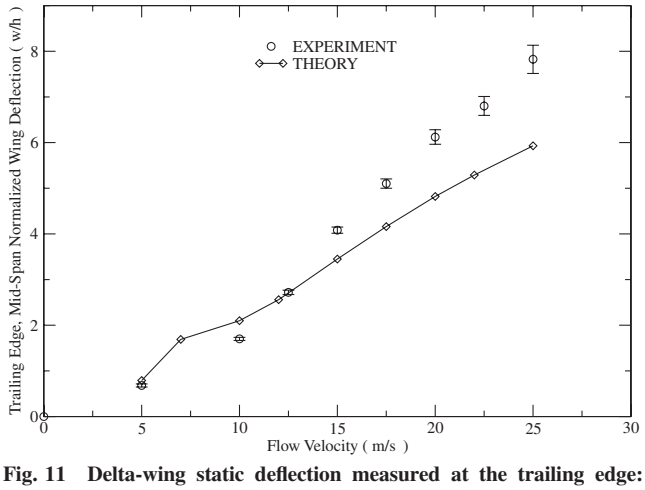

Fig. 11 Delta-wing static deflection measured at the trailing edge: midspan vs flow velocity for an angle of attack of 1 deg and a store location of $y/c = 0.545$.

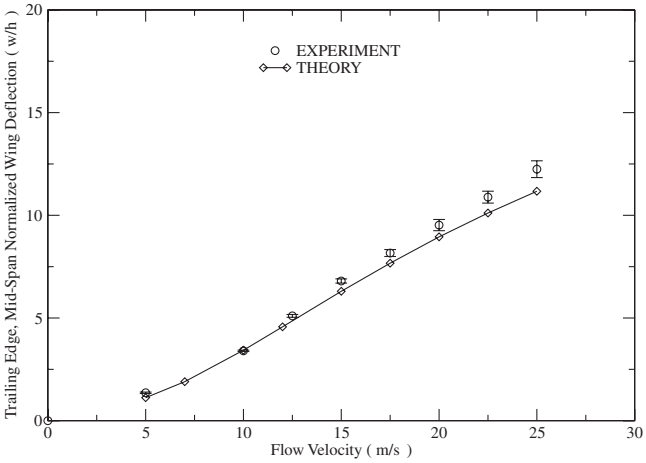

Fig. 12 Delta-wing static deflection measured at the trailing edge: midspan vs flow velocity for an angle of attack of 2 deg and a store location of $y/c = 0.545$.

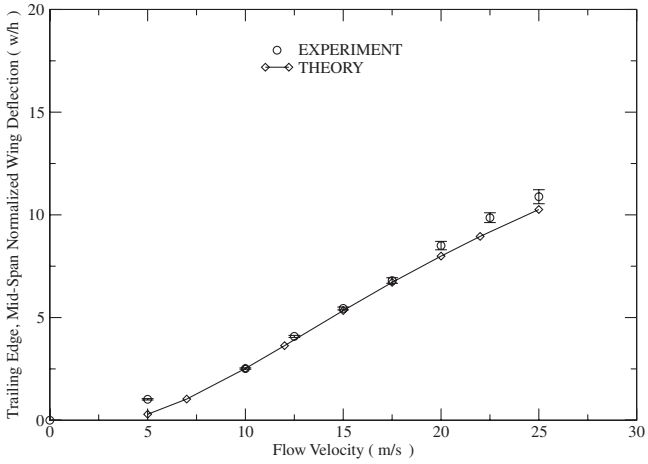

Fig. 14 Delta-wing static deflection measured at the trailing edge: midspan vs flow velocity for an angle of attack of −2 deg and a store location of $y/c = 0.545$.

velocities. However, the current model does a better job of qualitatively and quantitatively matching the experimental LCO results. Figure 16 is a plot of the delta-wing rms acceleration, measured at the wing trailing-edge midspan, as a function of the flow velocity for the case in which the store is located at $y/c = 0.545$. Shown on the plot are experimental LCO results for angles of attack of −2, −1, 0, 1, and 2 deg. Theoretical LCO results are only shown for 0- and 1-deg angles of attack. For all computed angles of attack, when compared with the results from the $y/c = 0.161$ configuration, the quantitative and qualitative agreement between theory and experiment is not as good.

IV. Conclusions

The flutter and LCO behavior of a 45-deg delta wing with various store configurations is studied using an aeroelastic model that includes a high-fidelity nonlinear finite element model for the structure and a vortex-lattice aerodynamic model for the wing flow dynamics. The store aerodynamics is modeled using slender-body theory. The results from this study are then compared with those computed in a previous study that used a lower-fidelity structural theory and to the experiment.

The zero-angle-of-attack flutter behavior of this delta wing with store is shown to be sensitive to the spanwise location of the store placement on the flexible wing. The zero-angle-of-attack flutter velocity and flutter frequencies computed using the current model compare favorably with both the experiment and the computational model used in [19].

At nonzero angle of attack, the flutter velocity of both the clean-wing configuration and the wing that had the store placed at a spanwise location of $y/c = 0.291$ did not show a great sensitivity to the angle of attack. This was both predicted by the current model and measured in the wind-tunnel experiments. Unlike the $y/c = 0.291$ store configuration, the experimental flutter data for the configuration that had the store at a spanwise location of $y/c = 0.545$ did show a good deal of sensitivity with respect to the angle of attack of the model. For an angle of attack of 2 deg, the wind-tunnel-model flutter velocity decreased by almost 20% when compared with the zero-angle-of-attack flutter velocity. This behavior was not predicted by the current computational model. It is possible that unmodeled nonlinear fluid dynamic effects may play an important role in causing this particular phenomena.

The zero-angle-of-attack LCO results computed with the current model compare well with the experiment for a store spanwise location of $y/c = 0.161$ and are both qualitatively and quantitatively better than those computed with the von Kármán model of [19]. At a store spanwise location of $y/c = 0.545$, the LCO results computed with the current model are not in as good of agreement with the experiment.

Perhaps the most interesting result reported in this work is the sensitivity of the flutter and LCO experimental (and, to some extent, computational) results for the wing-store configuration with the store located $y/c = 0.545$. For this configuration, the flutter-velocity results were shown to be extremely sensitive to the actual placement of the store and also to the angle of attack. A small deviation in either the store placement or angle of attack resulted in large changes in the

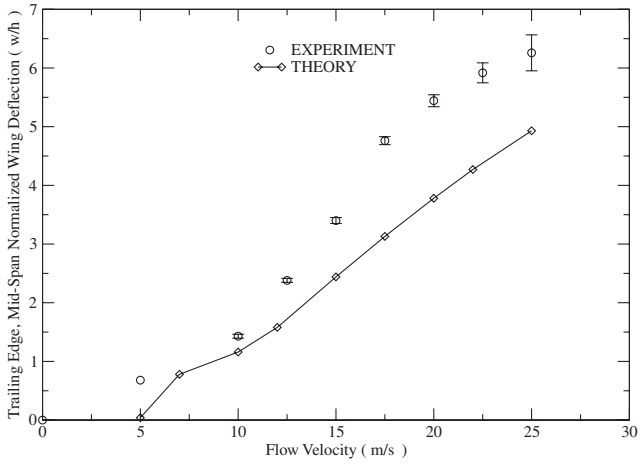

Fig. 13 Delta-wing static deflection measured at the trailing edge: midspan vs flow velocity for an angle of attack of −1 deg and a store location of $y/c = 0.545$.

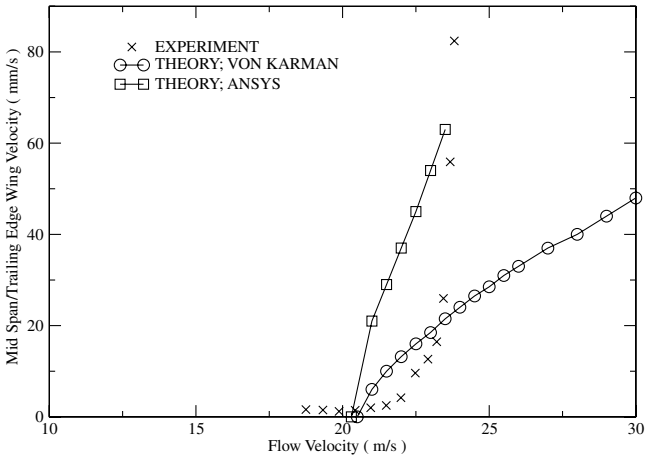

Fig. 15 Delta-wing tip LCO velocity vs flow velocity for zero angle of attack and a store position of $y/c = 0.161$.

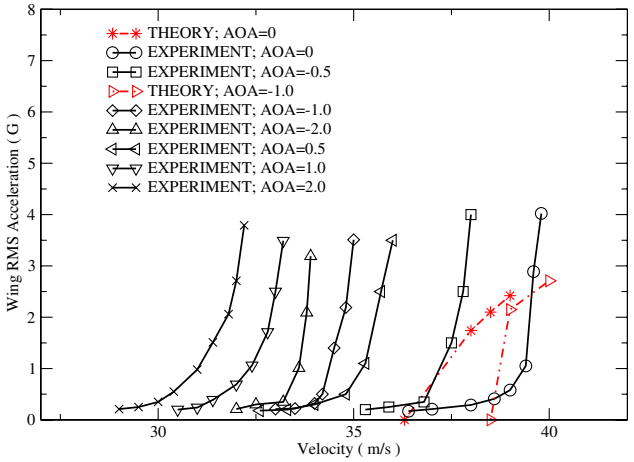

Fig. 16 Delta-wing rms acceleration measured at the wing trailing edge: midspan vs flow velocity for a store position of $y/c = 0.545$.

flutter velocity. Along with improvements in the aerodynamic model, further study for this particular configuration could include quantifying the effect, on flutter and LCO results, of uncertainty in the structural model and angle of attack.

Acknowledgments

This work was supported under two U.S. Air Force Office of Scientific Research (AFOSR) grants: "A Study of Uncertainties in Nonlinear Aeroelastic Systems" and "Theoretical Predictions of Limit Cycle Oscillations in Support of Flight Flutter Testing." The authors would like to thank Clark Allred of the AFOSR and Charles Denegri of Eglin Air Force Base for their advice and support of this work.

References

[1] Tang, D., Henry, J., and Dowell, E., "Limit Cycle Oscillations of Delta Wing Models in Low Subsonic Flow," *AIAA Journal*, Vol. 37, No. 11, 1999, pp. 1355–1362.

[2] Tang, D., and Dowell, E., "Effects of Angle of Attack on Nonlinear Flutter of a Delta Wing," *AIAA Journal*, Vol. 39, No. 1, 2001, pp. 15–21.

[3] Attar, P., Dowell, E., and White, J., "Modeling the LCO of a Delta Wing Using a High Fidelity Structural Model," AIAA Paper 2004-1402, Apr. 2004.

[4] Gordnier, R., "Computation of Limit Cycle Oscillations of a Delta Wing," AIAA Paper 2002-1411, Apr. 2002.

[5] Dowell, E., Hall, K., Thomas, J., Florea, R., Epureanu, B., and Heeg, J., "Reduced-Order Models in Unsteady Aerodynamics," AIAA Paper 1999-1261, Apr. 1999.

[6] Epureanu, B., Dowell, E., and Hall, K., "Reduced-Order Models of Unsteady Transonic Viscous Flows In Turbomachinery," *Journal of Fluids and Structures*, Vol. 14, No. 8, 2000, pp. 1215–1234. doi:10.1006/jfls.2000.0320

[7] Epureanu, B., Hall, K., and Dowell, E., "Reduced-Order Models of Unsteady Viscous Flows In Turbomachinery Using Viscous-Inviscid Coupling," *Journal of Fluids and Structures*, Vol. 15, No. 2, 2001, pp. 255–273. doi:10.1006/jfls.2000.0334

[8] Hall, K., Thomas, J., and Dowell, E., "Reduced-Order Modeling of Unsteady Small-Disturbance Flows Using a Frequency-Domain Proper Orthogonal Decomposition Technique," AIAA Paper 1999-0655, Jan. 1999.

[9] Thomas, J., Dowell, E., and Hall, K., "Nonlinear Inviscid Aerodynamic Effects on Transonic Divergence, Flutter and Limit Cycle Oscillations," *AIAA Journal*, Vol. 40, No. 4, Apr. 2002, pp. 638–646.

[10] Kholodar, D. B., Thomas, J. P., Dowell, E. H., and Hall, K. C., "A Parametric Study of Transonic Airfoil Flutter and Limit Cycle Oscillation Behavior," AIAA Paper 2002-1211, Apr. 2002.

[11] Thomas, J. P., Dowell, E. H., Hall, K. C., and Denegri, C. M., "Modeling Limit Cycle Oscillation Behavior of the F-16 Fighter Using a Harmonic Balance Approach," AIAA Paper 2004-1696, Apr. 2004.

[12] Beran, P., Khot, N., Eastep, F., Snyder, R., Zweber, J., Huttsell, L., and Scott, J., "The Dependence of Store-Induced Limit-Cycle Oscillation Predictions on Modelling Fidelity," Reduction of Military Vehicle Acquisition Time and Cost Through Advanced Modelling and Virtual Product Simulation Symposium, NATO Paper 44, Apr. 2002.

[13] Kim, K., and Strganac, T., "The Effects of External Stores on Nonlinear Aeroelastic Responses," AIAA Paper 2004-1942, Apr. 2004.

[14] Beran, P. S., Strganac, T. W., Kim, K., and Nichkawde, C., "Studies of Store-Induced Limit-Cycle Oscillations Using a Model with Full System Nonlinearities," *Nonlinear Dynamics*, Vol. 37, No. 4, September 2004, pp. 323–339. doi:10.1023/B:NODY.0000045544.96418.bf

[15] Chen, P., Lee, H., and Liu, D., "Unsteady Subsonic Aerodynamics for Bodies and Wings With External Stores Including Wake Effect," *Journal of Aircraft*, Vol. 30, No. 5, Sept.–Oct. 1993, pp. 618–628.

[16] Chen, P., Sulaeman, E., Liu, D., and Denegri, C., "Influence of External Store Aerodynamics on Flutter/LCO of a Fighter Aircraft," AIAA Paper 2002-1410, Apr. 2002.

[17] Mignolet, M., Liu, D., and Chen, P., "On the Nonlinear Structural Damping Mechanism of the Wing/Store Limit-Cycle Oscillation," AIAA Paper 1999-1459, Apr. 1999.

[18] Mignolet, M., Agelastos, A., and Liu, D., "Impact of Frictional Structural Nonlinearity in the Presence of Negative Aerodynamic Damping," AIAA Paper 2003-1428, Apr. 2003.

[19] Tang, D., Attar, P., and Dowell, E. H., "Flutter/Limit Cycle Oscillation Analysis and Experiment for Wing-Store Model," *AIAA Journal*, Vol. 44, July 2006, pp. 1662–1675. doi:10.2514/1.12634

[20] ANSYS, Software Package, Ver. 7.1, Swanson Analysis Systems, Inc., Canonsburg, PA, 2002.

[21] Nour-Omid, B., and Rankin, C., "Finite Rotation Analysis and Consistent Linearization Using Projectors," *Computer Methods in Applied Mechanics and Engineering*, Vol. 93, No. 3, 1991, pp. 353–384. doi:10.1016/0045-7825(91)90248-5

[22] Ashley, H., and Landahl, M., *Aerodynamics of Wings and Bodies*, Dover, New York, 1965.

[23] Katz, J., and Plotkin, A., *Low-Speed Aerodynamics*, 2nd ed., Cambridge Univ. Press, Cambridge, England, U.K., 2001.

[24] Bisplinghoff, R., Ashley, H., and Halfman, R., *Aeroelasticity*, Addison–Wesley, Cambridge, MA, 1995.

[25] Gordnier, R., and Visbal, M., "Development of a Three-Dimensional Viscous Aeroelastic Solver for Nonlinear Panel Flutter," *Journal of Fluids and Structures*, Vol. 16, No. 4, 2002, pp. 497–527. doi:10.1006/jfls.2000.0434

[26] Attar, P., Dowell, E., and Tang, D., "Theoretical and Experimental Investigation of the Effects of a Steady Angle of Attack on the Nonlinear Flutter of a Delta Wing Plate Model," *Journal of Fluids and Structures*, Vol. 17, No. 2, 2003, pp. 243–259. doi:10.1016/S0889-9746(02)00123-8

[27] Attar, P., Dowell, E., and White, J., "Modeling the LCO of a Delta Wing Using a High Fidelity Structural Model," *Journal of Aircraft*, Vol. 42, No. 5, Sept.–Oct. 2005, pp. 1209–1217. doi:10.2514/1.11325